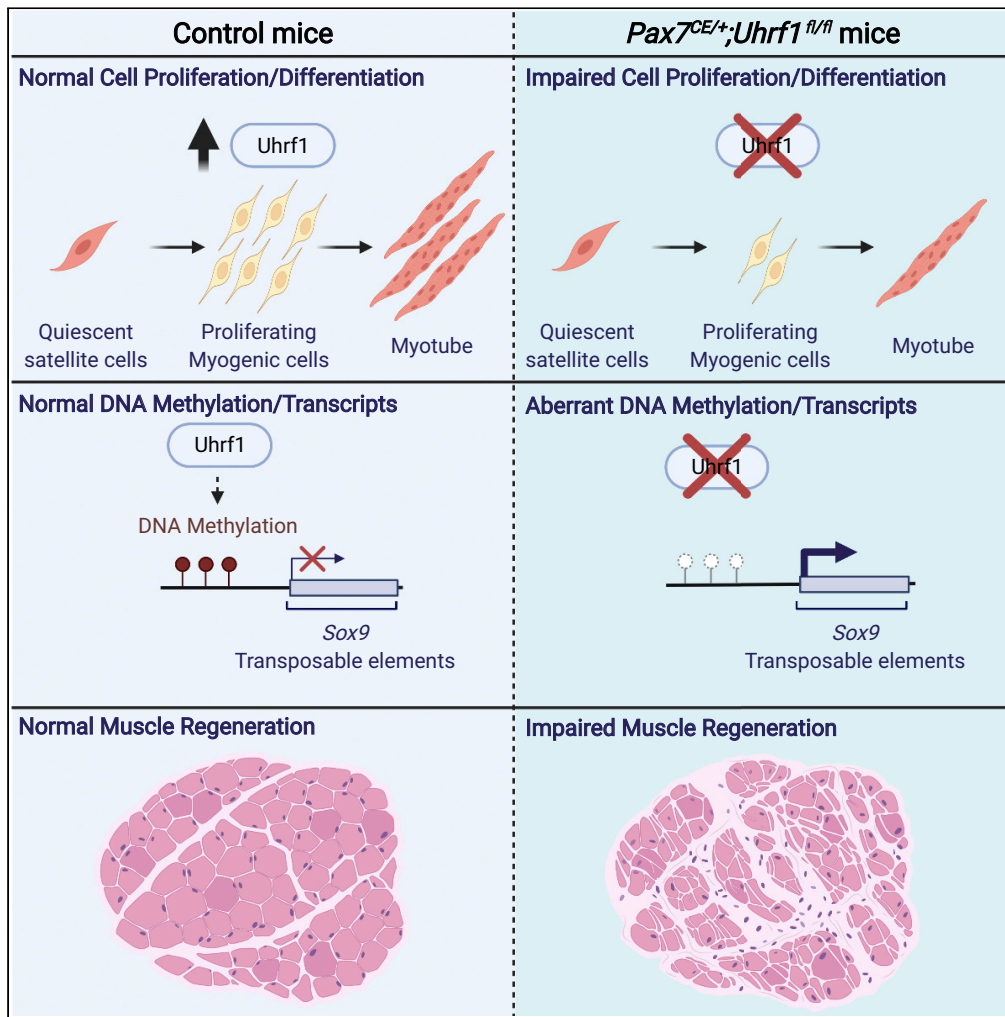


Article

Uhrf1 governs the proliferation and differentiation of muscle satellite cells



Hiroshi Sakai,
Yuichiro Sawada,
Naohito
Tokunaga, ...,
Tadahiko
Kikugawa, Takashi
Saika, Yuuki Imai

sakai.hiroshi.wh@ehime-u.ac.jp (H.S.)
y-imai@m.ehime-u.ac.jp (Y.I.)

Highlights

Uhrf1 is activated in proliferating myogenic cells

Uhrf1 in satellite cells is required for muscle regeneration

Ablation of Uhrf1 in satellite cells impairs their proliferation and differentiation

Uhrf1 controls cell-type-specific transcripts via maintenance of DNA methylation

Sakai et al., iScience 25, 103928
March 18, 2022 © 2022 The Author(s).
<https://doi.org/10.1016/j.isci.2022.103928>



Article

Uhrf1 governs the proliferation and differentiation of muscle satellite cells

Hiroshi Sakai,^{1,2,10,*} Yuichiro Sawada,^{3,10} Naohito Tokunaga,⁴ Kaori Tanaka,⁵ So Nakagawa,⁶ Iori Sakakibara,⁷ Yusuke Ono,⁸ So-ichiro Fukada,⁹ Yasuyuki Ohkawa,⁵ Tadahiko Kikugawa,³ Takashi Saika,³ and Yuuki Imai^{1,2,11,*}

SUMMARY

DNA methylation is an essential form of epigenetic regulation responsible for cellular identity. In muscle stem cells, termed satellite cells, DNA methylation patterns are tightly regulated during differentiation. However, it is unclear how these DNA methylation patterns affect the function of satellite cells. We demonstrate that a key epigenetic regulator, ubiquitin like with PHD and RING finger domains 1 (Uhrf1), is activated in proliferating myogenic cells but not expressed in quiescent satellite cells or differentiated myogenic cells in mice. Ablation of Uhrf1 in mouse satellite cells impairs their proliferation and differentiation, leading to failed muscle regeneration. Uhrf1-deficient myogenic cells exhibited aberrant upregulation of transcripts, including Sox9, with the reduction of DNA methylation level of their promoter and enhancer region. These findings show that Uhrf1 is a critical epigenetic regulator of proliferation and differentiation in satellite cells, by controlling cell-type-specific gene expression via maintenance of DNA methylation.

INTRODUCTION

Adult skeletal muscle has a great capacity for regeneration, which is mediated by muscle satellite (stem) cells that express the *Pax7* gene (Seale et al., 2000). Genetic ablation of Pax7-expressing satellite cells in mice led to a drastic loss of muscle tissue and loss of muscle regeneration (Lepper et al., 2011; McCarthy et al., 2011; Murphy et al., 2011; Sambasivan et al., 2011). During regeneration, satellite cells are rapidly activated to proliferate and give rise to myoblasts that fuse to form new skeletal muscle fibers. Although it has been reported that many intrinsic and extrinsic cell signals contribute to the maintenance, activation, and differentiation of satellite cells, little information is available on the role of epigenetic regulation, especially maintenance of DNA methylation patterns, in satellite cells during muscle regeneration.

DNA methylation is critical for regulating gene transcription. Several studies reported that DNA methylation patterns are altered during the proliferation and differentiation of mouse and human myogenic cells (Carrío et al., 2015; Miyata et al., 2015; Tsumagari et al., 2013). A family of DNA methyltransferases (DNMT) mediates DNA methylation by enzymatic activities including *de novo* methylation (catalyzed by DNMT3a and DNMT3b) or maintenance of methylation (by DNMT1). Deleting DNMT3a in satellite cells led to loss of proliferation with increased expression of the *Cdkn1c* (Naito et al., 2016) or the *Gdf5* gene (Hatazawa et al., 2018). Further, we reported that deletion of *Dnmt1* in satellite cells impaired muscle regeneration *in vivo*, resulting in a reduced number of myogenic cells *in vitro* (Iio et al., 2021). Thus, identification of epigenetic regulator is important to understand the mechanisms by which DNA methylation governs the proliferation and differentiation of satellite cells.

Ubiquitin like with PHD and RING finger domains 1 (Uhrf1; also known as Np95 in mice and ICB90 in humans), acts as an epigenetic regulator; it is essential for maintenance of DNA methylation by recruiting DNMT1 to hemi-methylated DNA sites (Bostick et al., 2007; Sharif et al., 2007), and it also can interact with DNMT3a and DNMT3b (Meilinger et al., 2009). Consistently, UHRF1 is upregulated in proliferating cells, such as neural stem cells and basal stem cells in the airway, and downregulated during differentiation or quiescence (Ramesh et al., 2016; Xiang et al., 2017). Previous reports have shown that ablation of *Uhrf1* in different cell types, including embryonic stem cells (Sharif et al., 2007), T cells (Obata et al., 2014), hematopoietic stem cells (Zhao et al., 2017), chondrocytes (Yamashita et al., 2018), and adult neural stem cells (Blanchart et al., 2018), leads to DNA hypomethylation, resulting in abrogation of proliferation and/or differentiation. However, no information is available on the functions of *Uhrf1* in satellite cells in muscle

¹Division of Integrative Pathophysiology, Proteo-Science Center, Ehime University, Toon, Ehime 791-0295, Japan

²Department of Pathophysiology, Ehime University Graduate School of Medicine, Toon, Ehime 791-0295, Japan

³Department of Urology, Ehime University Graduate School of Medicine, Toon, Ehime 791-0295, Japan

⁴Division of Analytical Biomedicine, Advanced Research Support Center, Ehime University, Toon, Ehime 791-0295, Japan

⁵Division of Transcriptomics, Medical Institute of Bioregulation, Kyushu University, Higashi-ku, Fukuoka 812-0054, Japan

⁶Department of Molecular Life Science, Tokai University School of Medicine, Isehara, Kanagawa 259-1193, Japan

⁷Department of Nutritional Physiology, Institute of Medical Nutrition, Tokushima University Graduate School, Kuramoto-cho, Tokushima 770-8503, Japan

⁸Department of Muscle Development and Regeneration, Institute of Molecular Embryology and Genetics, Kumamoto University, Honjo, Kumamoto 860-0811, Japan

⁹Project for Muscle Stem Cell Biology, Graduate School of Pharmaceutical Sciences, Osaka University, Suita, Osaka 565-0871, Japan

¹⁰These authors contributed equally.

¹¹Lead contact

*Correspondence: sakai.hiroshi.wh@ehime-u.ac.jp (H.S.), y-imai@m.ehime-u.ac.jp (Y.I.)
<https://doi.org/10.1016/j.isci.2022.103928>



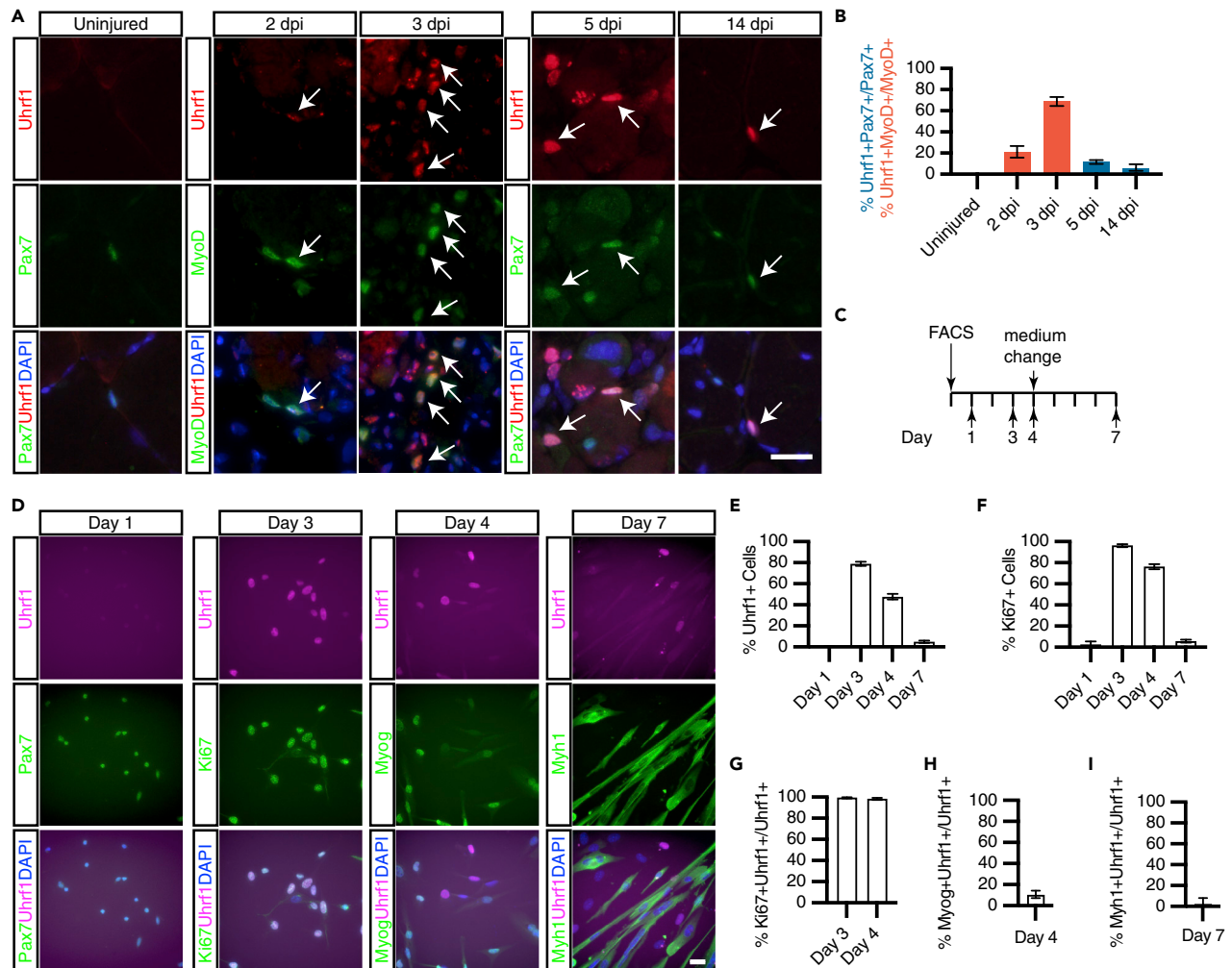


Figure 1. Uhrf1 is active in myogenic cells after muscle injury and during *in vitro* culture

(A) Immunostaining of Pax7, MyoD, and Uhrf1 during muscle regeneration. Arrows show Uhrf1+Pax7+ or Uhrf1+MyoD+ cells.

(B) Quantification of Uhrf1+ cells among Pax7+ or MyoD+ cells in uninjured and injured TA muscles collected at 2, 3, 5, and 14 dpi.

(C) Time course of myogenic cells cultured *in vitro*.

(D) Immunostaining of Uhrf1, Pax7, Ki67, Myogenin, and Myh1 after 1, 3, 4, and 7 days of culture.

(E) Quantification of Uhrf1+ cells *in vitro*.

(F) Quantification of proliferating (Ki67+) cells *in vitro*.

(G) Quantification of Ki67+ cells among Uhrf1+ cells after 3 or 4 days of culture.

(H) Quantification of Myogenin+ cells among Uhrf1+ cells after 4 days of culture.

(I) Quantification of Myh1+ cells in Uhrf1+ fibers after 7 days of culture. For all graphs, data were pooled from three or four independent experiments and are expressed as the mean with 95% CI. Scale bars: 20 μ m. See also [Figure S1](#)

regeneration. Here, we investigated the expression pattern and function of *Uhrf1* within satellite cells and their progeny *in vivo* and *in vitro* by using satellite cell-specific *Uhrf1* knockout mice.

RESULTS

Uhrf1 is active in myogenic cells after muscle injury and during *in vitro* culture

To determine whether and when *Uhrf1* is expressed in muscles, the tibialis anterior (TA) muscles were injured by cardiotoxin (CTX) injection; uninjured and injured TA muscles were collected on different days postinjury (dpi). During muscle regeneration, the *Uhrf1* transcript level peaked at 4 dpi and then decreased by 14 dpi ([Figure S1A](#)). To determine which myogenic cells contain active *Uhrf1*, immunofluorescence staining of *Uhrf1*, Pax7, and MyoD was performed in TA muscle sections ([Figure 1A](#)). In uninjured TA

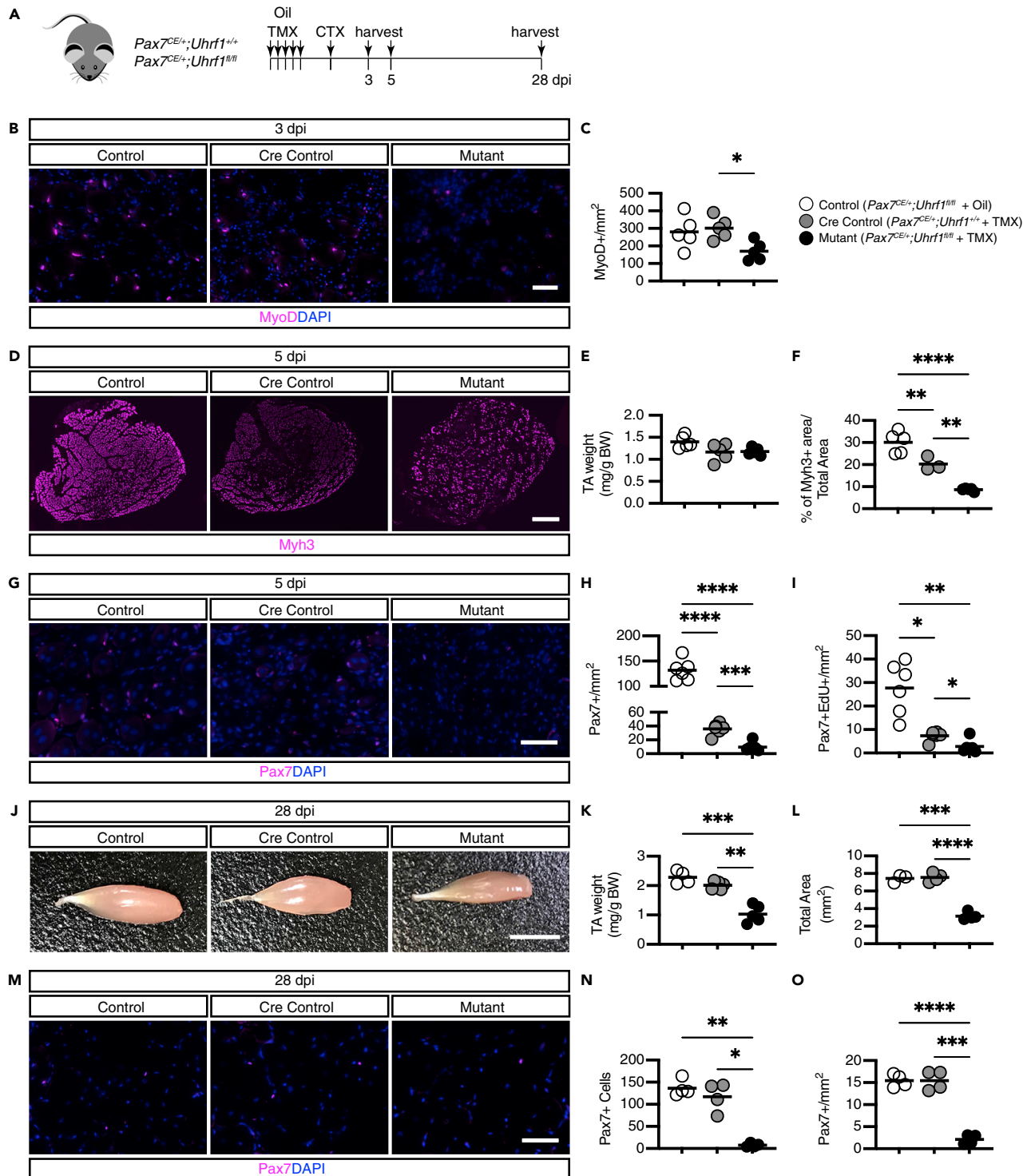


Figure 2. Loss of Uhrf1 expression in satellite cells impairs muscle regeneration
 (A) Experimental design for TMX treatment followed by CTX injection and sample harvest.
 (B) Immunostaining of MyoD in TA muscles at 3 dpi.
 (C) Quantification of MyoD⁺ cells at 3 dpi (n = 5 mice/condition).
 (D) Immunostaining of Myh3 in TA muscles at 5 dpi.
 (E) Mass of TA muscles at 5 dpi (n = 5 mice/condition).

Figure 2. Continued

- (F) The average area of Myh3+ regenerating myofibers in TA muscle cross-sections at 5 dpi (n = 3 or 5 mice/condition).
 (G) Immunostaining of Pax7 in TA muscle cross-sections at 5 dpi.
 (H) Quantification of Pax7+ cells at 5 dpi (n = 6 mice/condition).
 (I) Quantification of Pax7+EdU+ cells at 5 dpi (n = 6 mice/condition).
 (J) Whole-mount TA at 28 dpi.
 (K) Mass of TA muscles at 28 dpi (n = 4 or 5 mice/condition).
 (L) The average total area of TA muscle cross-sections at 28 dpi (n = 3 or 4 mice/condition).
 (M) Immunostaining of Pax7 in TA muscle cross-sections at 28 dpi.
 (N and O) The total and average number of Pax7+ cells in TA muscle cross-sections at 28 dpi (n = 4 mice/condition). Statistical significance was determined by Welch's ANOVA with Dunnett's T3 multiple comparison test. *p < 0.05, **p < 0.01, ***p < 0.001, ****p < 0.0001. Scale bars: 50 μm in (B, G, and M), 500 μm in (D), and 5 mm in (J). See also [Figure S2](#)

muscles, almost none of the Pax7+ satellite cells expressed Uhrf1 ([Figure 1B](#)). Although only 21% of MyoD+ cells were Uhrf1+ at 2 dpi, about 70% of MyoD+ cells expressed Uhrf1 at 3 dpi, when the number of myogenic cells peaked ([Ogawa et al., 2014](#)). At 5 dpi, when the number of Pax7+ cells peaked during normal regeneration postinjury ([Murphy et al., 2011](#)), 11% of Pax7+ cells expressed Uhrf1, and this percentage decreased to 5.8% at 14 dpi ([Figure 1B](#)), which was compatible with the Uhrf1 transcript level in injured TA muscles. More EdU+ cells were found in Pax7+Uhrf1+ cells than Pax7+Uhrf1- cells at 5 dpi ([Figure S1B](#)), indicating Uhrf1 is expressed in proliferating myogenic cells. In addition, *Uhrf1* expression gradually decreased after induction of differentiation in C2C12 cells ([Figures S1C–S1E](#)).

To further examine the expression pattern of Uhrf1, satellite cells were isolated by FACS and cultured for up to 7 days *in vitro* ([Figure 1C](#)). Almost all cells were positive for Pax7 on day 1, but none of these cells expressed Uhrf1 ([Figure 1D](#)), which supported the *in vivo* results in intact muscles. The majority of myogenic cells (78%) were positive for Uhrf1 on day 3, and this percentage gradually decreased during differentiation ([Figure 1E](#)). The expression pattern of Ki67+ proliferation cells was similar to that of Uhrf1+ cells ([Figure 1F](#)). Whereas almost all Uhrf1+ cells expressed Ki67 on day 3 and 4 ([Figure 1G](#)), only 10% of Uhrf1+ cells expressed Myogenin on day 4 ([Figure 1H](#)), and almost no Uhrf1+ cells expressed Myh1 on day 7 ([Figure 1I](#)). These observations indicate that Uhrf1 is not expressed in satellite cells during quiescence but is transiently expressed in proliferating myogenic cells before being downregulated during differentiation.

Loss of Uhrf1 expression in satellite cells impairs muscle regeneration

To determine whether *Uhrf1* expression in satellite cells and their progeny is necessary for muscle regeneration, we selectively deleted this gene using *Pax7^{Cre/+}* ([Lepper et al., 2009](#)) and *Uhrf1^{fl/fl}* ([Skarnes et al., 2011](#)) mice. The efficiency of *Uhrf1* ablation in satellite cells and their progeny was measured by isolating satellite cells by FACS from hindlimb muscles of *Pax7^{Cre/+};Uhrf1^{fl/fl}* mice following administration of oil (control mice), *Pax7^{Cre/+}* mice following administration of tamoxifen (TMX, Cre control mice), or *Pax7^{Cre/+};Uhrf1^{fl/fl}* mice following administration of TMX (mutant mice) for 5 consecutive days ([Figures S2A and S2B](#)). Deletion was highly efficient, as the Uhrf1 transcript and protein level was 90% lower in mutant mice than Cre control myogenic cells ([Figures S2C and S2D](#)). Together, these experiments indicate that Uhrf1 expression was effectively abolished in satellite cells and their progeny from *Pax7^{Cre/+};Uhrf1^{fl/fl}* mice.

To investigate the effects of Uhrf1 expression loss in satellite cells and their progeny on intact muscle and during muscle regeneration, the TA muscles of controls and mutant mice were injured by CTX and harvested at 3 and 5 dpi ([Figure 2A](#)). Because *Pax7^{Cre/+}* mice treated with TMX (Cre control mice) exhibit a mild muscle regeneration phenotype ([Lahmann et al., 2021](#); [Mademtoglou et al., 2018](#); [Sakai et al., 2020](#)), Cre control mice were included in the experiments for regeneration. There was no change in muscle mass or the number of Pax7+ cells in uninjured TAs of each mouse ([Figures S2E–S2G](#)), because quiescent satellite cells originally lack the expression of Uhrf1 ([Figure 1D](#)). At 3 dpi, there was a significant decrease in the number of MyoD+ cells in mutant mice ([Figures 2B and 2C](#)), indicating a decrease in myogenic cells. The regenerating fibers, characterized by expression of embryonic myosin heavy chain (Myh) 3, were detected at 5 dpi in control mice ([Figure 2D](#)), similar to a previous report ([Murphy et al., 2011](#)). Although there was no difference in the muscle mass ([Figure 2E](#)), the Myh3 level was decreased in Cre control mice compared with the control, whereas the proportion of Myh3+ regenerating fibers was severely reduced in mutant mice ([Figure 2F](#)). These results indicate that loss of *Uhrf1* affects the regeneration of new fibers.

In addition, there was a significant decrease in the number and proliferation of Pax7+ cells (Figures 2G–2I) at 5 dpi in mutant mice compared with control and Cre control mice.

To determine whether the observed phenotype in the early phase of the muscle regeneration was sustained during the process, injured TA muscles were harvested at 28 dpi (Figure 2A), at which time regeneration is largely complete (Murphy et al., 2011). Although there was no difference in the TA muscle mass between control and Cre control muscle according to macroscopic observations (Figure 2J), the mutant mice exhibited significant muscle mass loss in the TA muscles (Figure 2K). There was a significant decrease in the total CSA in mutant mice (Figures 2L and S2H) but no difference between the control and Cre control mice. Also, TA sections contained a significantly lower number of Pax7+ cells in mutant mice compared with control mice (Figures 2M and 2N), and this significant decrease remained even after normalization to the total CSA (Figure 2O). In summary, loss of Uhrf1 expression in satellite cells significantly impaired their proliferation and muscle regeneration.

Uhrf1 deficiency in satellite cells disturbs proliferation and differentiation of myogenic cells *in vitro*

To investigate the mechanisms of satellite cell impairment in $Pax7^{CE/+};Uhrf1^{fl/fl}$ mice, single myofibers were isolated from the extensor digitorum longus muscle of control and mutant mice and cultured for up to 4 days (Figure S3A). On days 0 and 2, the number of Pax7+ cells per myofiber was comparable between the mutant and control mice (Figure S3B). In contrast, the total number of myogenic cells and the proportion of Pax7-MyoD+ myoblasts on day 4 were decreased in the myofibers of mutant mice compared with control mice (Figure S3B).

To further characterize the impaired proliferation and differentiation observed in culture, satellite cells from control, Cre control, and mutant mice were characterized *in vitro* (Figure 3A). Uhrf1 protein was expressed in 65% of myogenic cells cultured for 3 days from both control and Cre mice but in 5.2% of those from mutant mice (Figures S3C and S3D), demonstrating efficient deletion of Uhrf1 allele in isolated myogenic cells. In EdU labeling experiments to assess proliferation, although Cre control myogenic cells reduced proliferation compared with control mice, only 24% of myogenic cells were positive for EdU in mutant mice, compared with approximately 40% in Cre control mice, on day 3 (Figures 3B and 3C). Furthermore, the number of Myogenin+ cells was significantly decreased in mutant mice on day 4 (Figures 3D and 3E). In addition, myotube formation, observed by Myh1 staining on day 7, was also compromised in the mutant mouse cells (Figures 3F and 3G). Taken together, these *in vitro* findings indicate that Uhrf1 is required in myogenic cells for proliferation and the loss of Uhrf1 leads to impairments of differentiation.

Loss of Uhrf1 in satellite cells alters DNA methylation patterns and subsequently transcriptional programs

To identify the genes affected by Uhrf1 deficiency in satellite cells and their progeny, RNA-Seq was performed in cultured myogenic cells obtained from control, Cre control, and mutant mice (Figure 4A). Because a heatmap of the expression profiles showed a clear distinction between the control and Cre control myogenic cells (Figure S4A), we focused on the comparison between Cre control and mutant myogenic cells for further analysis (Figure 4B). We detected 3,644 upregulated and 3,672 downregulated genes in the mutant compared with Cre control myogenic cells. According to Gene Ontology (GO) enrichment analysis, the downregulated genes showed significant enrichment of the biological process terms related to cell proliferation and cell cycle (Figure 4C), consistent with the impairment of these processes observed in the mutant cells. The genes that were upregulated in mutant myogenic cells showed enrichment of myogenesis-independent GO terms such as “positive regulation of smooth muscle cell migration” and “blood vessel development.” Because no caspase in the critical apoptotic signaling pathway was upregulated in the mutant cells (Table S1), the activation of apoptosis may not be a main cause of the phenotype of the mutant cells. In addition, gene sets associated with transposable elements (TEs), such as “regulation of transposition,” was also enriched among the upregulated genes (Figure 4C). As loss of DNA methylation due to Uhrf1 deficiency in embryonic stem cells (Sharif et al., 2007) or neural stem cells (Ramesh et al., 2016) leads to activation of TEs, we thus examined the expression of TEs using RNA-Seq data by STAR program (v2.7.6a) (Dobin et al., 2013) with dedicated parameters and algorithms for TE analysis (see STAR Methods). We found upregulation of intracisternal A particles (IAPs) in mutant compared with Cre control myogenic cells (Figure 4D), which is in line with the results from *Uhrf1*-deficient embryonic stem cells (Bostick et al., 2007; Sharif et al., 2007).

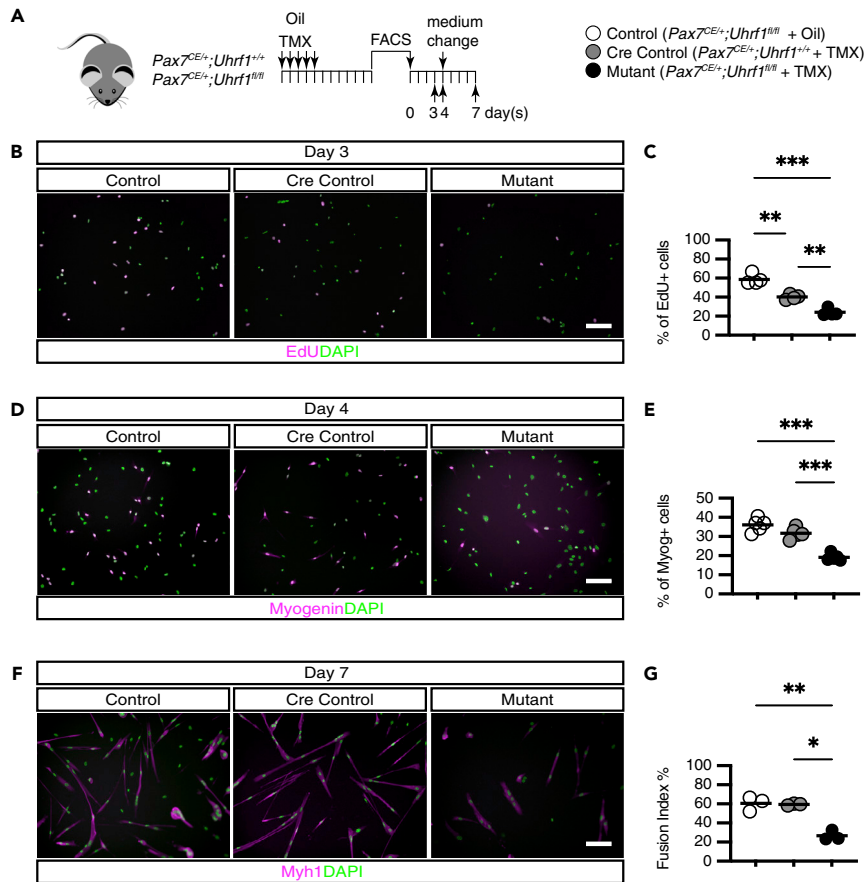


Figure 3. Uhrf1 deficiency in satellite cells disturbs proliferation and differentiation of myogenic cells in vitro

(A) Experimental design for TMX followed by FACS and immunostaining after 3, 4, and 7 days in culture.
 (B) EdU detection in myogenic cells after 3 days in culture.
 (C) Quantification of EdU+ cells after 3 days in culture (n = 4 mice/condition).
 (D) Immunostaining of Myogenin after 4 days in culture.
 (E) Quantification of Myogenin+ cells after 4 days in culture (n = 5 mice/condition).
 (F) Immunostaining of Myh1 after 7 days in culture.
 (G) Fusion index after 7 days in culture (n = 3 mice/condition). Statistical significance was determined by Welch's ANOVA with Dunnett's T3 multiple comparison test. *p < 0.05, **p < 0.01, ***p < 0.001. Scale bars: 100 μ m. See also [Figure S3](#)

To determine whether the genes upregulated by Uhrf1 deficiency were specific to myogenic cells, we compared the upregulated genes in chondrocytes (Yamashita et al., 2018) and hematopoietic stem cells lacking Uhrf1 (Zhao et al., 2017) with those in myogenic cells (Figure S4B). Among the 3,644 genes upregulated in Uhrf1 deficient-myogenic cells, 436 overlapped with the 1,122 genes upregulated in Uhrf1-knockout chondrocytes. On the other hand, only 82 genes overlapped with the 626 genes upregulated in hematopoietic stem cells lacking Uhrf1. These results indicate that Uhrf1 deficiency induces upregulation of partially overlapped common genes regardless of cell types, but cell-specific knockout of Uhrf1 may lead to upregulation of cell-specific genes by disruption of cell-type-specific maintenance DNA methylation mechanisms.

We next performed methyl-CpG-binding domain protein-2-enriched genome sequencing (MBD2-Seq) in the control and mutant cultured myogenic cells (Figure 4A). The higher GC count per read in methylated DNA compared with unmethylated DNA (Figure S4C) and the distinct methylation patterns observed at the H19 and Kcnq1ot1 loci, which are imprinted genes (Figure S4D), indicated proper enrichment of methylated DNA by MBD2. To identify DNA loci methylated by Uhrf1, peak calling was performed using MACS2. We identified 45,582 peaks, and these loci were enriched in promoters, downstream regions, and gene bodies of the genome (Figure 4E). To identify Uhrf1 target genes in myogenic cells, we analyzed

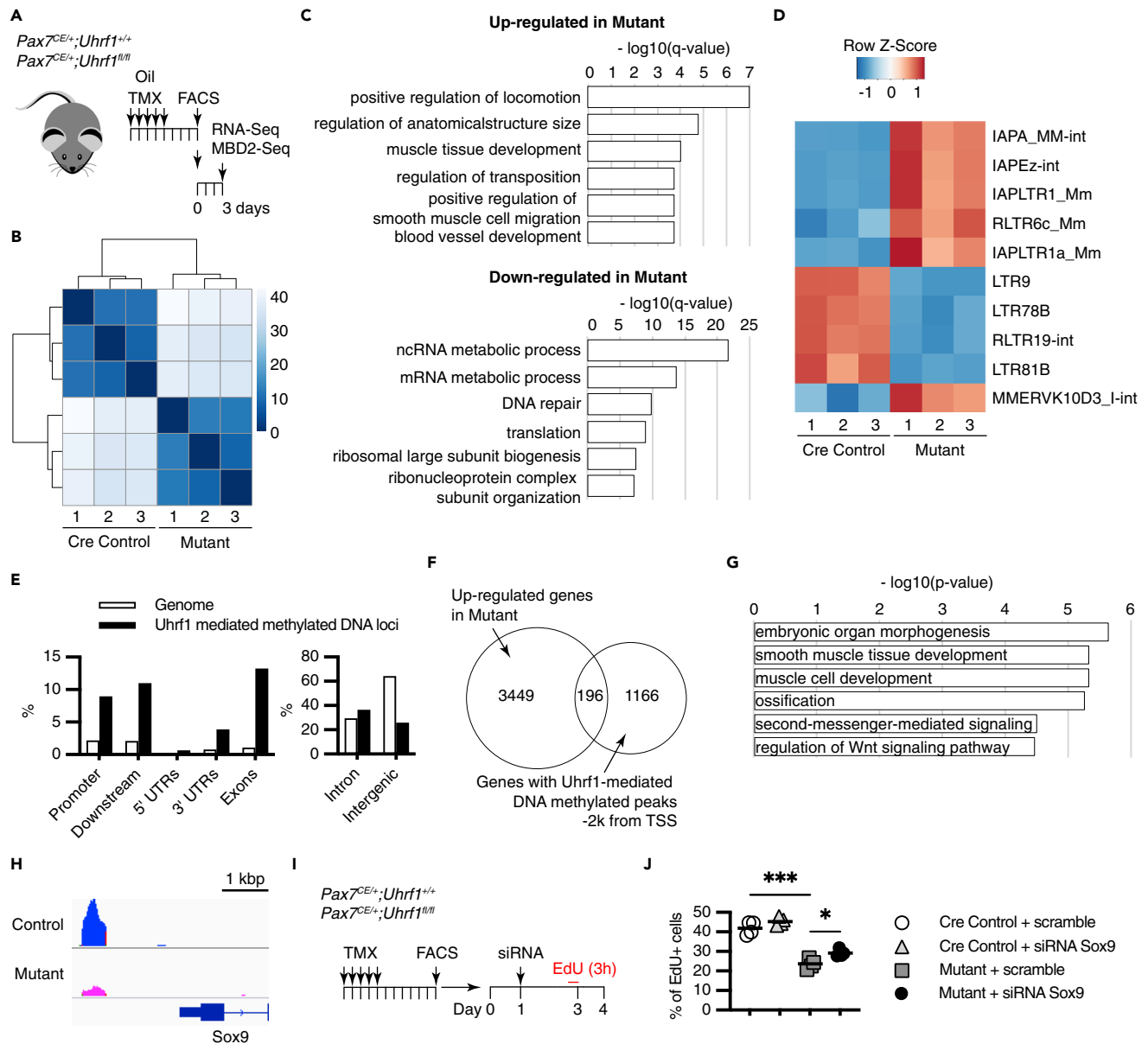


Figure 4. Loss of Uhrf1 in satellite cells alters DNA methylation patterns and subsequently transcriptional programs

(A) Experimental design for RNA-Seq and MBD2-Seq.
 (B) Heatmap of expression similarity between Cre control and mutant samples.
 (C) Bar graph of the Gene Ontology (GO) terms enriched among the upregulated and downregulated genes in mutant myogenic cells.
 (D) Heatmap showing the RNA-Seq Z score of top 10 differentially expressed retrotransposon families.
 (E) Distribution of Uhrf1-mediated methylated DNA with the given intervals and scores, with the genomic features determined using a cis-regulatory element annotation system.
 (F) Venn diagram of the upregulated genes associated with Uhrf1-mediated methylated DNA loci.
 (G) Bar graph of the GO terms enriched among the upregulated genes associated with Uhrf1-mediated methylated DNA loci.
 (H) Methylated DNA signals around the Sox9 loci in control and mutant myogenic cells visualized using IGV.
 (I) Experimental design for the siRNA treatments.
 (J) Quantification of EdU+ Sox9-knockdown myogenic cells (n = 4 mice/condition). Statistical significance was determined by Welch's ANOVA with Dunnett's T3 multiple comparison test. *p < 0.05, ***p < 0.001. See also Figure S4.

the genes upregulated by *Uhrf1* deficiency that overlapped with the Uhrf1-mediated DNA methylated peaks. We found 196 genes with Uhrf1-mediated peaks within -2000 bp from the transcriptional start site (Figure 4F). GO enrichment analysis showed that myogenesis-independent gene sets, such as

“embryonic organ morphogenesis,” “smooth muscle tissue development,” and “ossification,” were enriched in these genes (Figures 4G and S4F).

Among these genes, *Sox9*, which is a key transcription factor in chondrocytes differentiation and skeletal development (Bi et al., 1999), was associated with all of the top six GO categories. We also detected reduced DNA methylation levels in the regions upstream of the *Sox9* loci in mutant myogenic cells (Figure 4H). This region is annotated as proximal enhancer by the ENCODE (Consortium et al., 2020) and overlapped with H3K4me1 peaks, indicating the primed enhancer, in MC3T3-E1 osteoblastic cell line expressing *Sox9* (Figure S4E) (Oki et al., 2018). To explore whether upregulation of *Sox9* is responsible for the impaired proliferation and differentiation of *Uhrf1*-deficient myogenic cells, we treated mutant myogenic cells with siRNA targeting *Sox9* (Figure 4I). Knockdown of *Sox9* (Figure S4G) significantly rescued the impaired proliferation of the mutant myogenic cells (Figures 4J and S4H). However, *Sox9* knockdown was not sufficient to rescue the impaired differentiation of the mutant myogenic cells (Figures S4I and S4J). Taken together, *Uhrf1*-mediated DNA methylation in satellite cells and their progeny controls specific gene expression in a cell-type-specific manner and negatively regulates the aberrant expression of genes that can induce the differentiation toward other cell type, such as *Sox9*, for physiological proliferation and/or differentiation of satellite cells.

DISCUSSION

In this study, we identified *Uhrf1* as a critical regulator of skeletal muscle satellite cells. Notably, *Uhrf1* is not expressed during quiescence but is upregulated during proliferation and downregulated during differentiation in satellite cells. Our findings agree with previous reports showing that *Uhrf1* is necessary for maintaining the DNA methylation profile during DNA replication in proliferating cells and downregulated during differentiation or quiescence other than satellite cells (Ramesh et al., 2016; Xiang et al., 2017). As *Uhrf1* overexpression was reported to contribute to cancer initiation and progression (Mudbhary et al., 2014), tight regulation of *Uhrf1* expression in stem cells appears to be critical for self-renewal and differentiation.

Further, ablation of *Uhrf1* in satellite cells led to impaired muscle regeneration, similar to *Dnmt1*- (Iio et al., 2021) or *Dnmt3a*-deficient mice (Naito et al., 2016). The marked loss of EdU incorporation indicated a remarkable reduction in the number of *Uhrf1*-deficient myogenic cells *in vitro* and *in vivo* at 28 dpi. Therefore, the impairment of muscle regeneration of mutant mice could result from decreased numbers of myogenic cells.

In addition, we report that loss of *Uhrf1* in satellite cells alters transcriptional programs caused by alteration of genome-wide DNA methylation patterns. Consistent with the impaired proliferation of *Uhrf1*-deficient myogenic cells, we found that many cell-cycle-related genes were downregulated. We propose that *Uhrf1* deficiency in mutant myogenic cells results directly in hypomethylation and abnormal upregulation of transcriptions. Indeed, the GO term enriched among the upregulated genes by hypomethylation in *Uhrf1*-deficient myogenic cells was myogenesis independent such as “embryonic organ morphogenesis” and “smooth muscle tissue development.” As satellite cells have a potential to adopt a pericyte phenotype following stimulation of the Notch and PDGF signaling pathways (Gerli et al., 2019), loss of *Uhrf1* in satellite cells might trigger partial transdifferentiation into vascular-like cells. We found that TEs, especially IAPs, were strongly upregulated in *Uhrf1*-deficient myogenic cells. This phenotype is comparable with that of *Uhrf1*-deficient cortical neural stem cells showing strong activation of IAPs (Ramesh et al., 2016). Because long-terminal repeats in IAPs could change gene regulation at a given locus (Morgan et al., 1999), further studies are needed to clarify whether transposition of IAPs into new genomic loci would contribute to the phenotype of mutant satellite cells.

Finally, we found the aberrant expression of *Sox9*, which is a transcription factor that is essential for chondrocyte differentiation and cartilage formation, in mutant myogenic cells with the reduction of DNA methylation at its proximal enhancer. We showed that suppression of the increased *Sox9* in *Uhrf1*-deficient myogenic cells partially rescued their impaired proliferation. These results are congruent with the report showing that *Sox9* overexpression in chondrocytic cells suppress their cell cycle (Panda et al., 2001). The fact that *Sox9*-expressing chondrocytes and skeletal muscle cells share a developmental origin as somites (Lagha et al., 2008) might have influenced the aberrant expression of *Sox9* in *Uhrf1*-deficient myogenic cells. Thus, we propose that *Uhrf1* epigenetically governs, at least in part, appropriate gene expression and suppression in satellite cells for their ideal proliferation and differentiation.

In conclusion, the present study points Uhrf1 as a regulator of self-renewal and differentiation of satellite cells via genome-wide DNA methylation patterning.

Limitations of the study

Knockdown of Sox9 partly rescued the impaired proliferation but not the differentiation of *Uhrf1*-deficient myogenic cells. Therefore, other factors or mechanisms, including not only the transcripts regulated by Uhrf1 but also the chromatin state such as histone modifications, can also regulate the behavior of mutant myogenic cells. Considering the enrichment of GO terms such as "DNA repair" in downregulated genes in mutant myogenic cells, the genome instability seems to be one of the mechanisms for explaining the phenotype of mutant myogenic cells. In addition, we found a number of phenotypes in *Uhrf1*-deficient myogenic cells overlapped with *Dnmt1*-deficient ones (Iio et al., 2021). Further efforts to perform the integrated analysis of omics data, including histone modifications, of *Uhrf1*- and *Dnmt1*-deficient myogenic cells may help understand the different roles between Uhrf1 and Dnmt1 for regulating satellite cells.

STAR★METHODS

Detailed methods are provided in the online version of this paper and include the following:

- KEY RESOURCES TABLE
- RESOURCE AVAILABILITY
 - Lead contact
 - Materials availability
 - Data and code availability
- EXPERIMENTAL MODEL AND SUBJECT DETAILS
 - Animals
 - Cell lines
 - Primary cell cultures
- METHOD DETAILS
 - Immunofluorescence and microscopy
 - Isolation of skeletal muscle-derived mononuclear myogenic cells
 - Western blotting
 - siRNA transfection
 - EdU labelling and detection
 - RNA isolation and quantitative real-time PCR
 - Isolation, culture, and immunostaining of single myofibers
 - RNA-Seq and data analysis
 - MBD2-Seq and analysis of the sequencing data
- QUANTIFICATION AND STATISTICAL ANALYSIS

SUPPLEMENTAL INFORMATION

Supplemental information can be found online at <https://doi.org/10.1016/j.isci.2022.103928>.

ACKNOWLEDGMENTS

We thank S. Tajbakhsh for critically reading the manuscript, S. Nakanishi and A. Nishio for their technical support, K. Kameda for the flow cytometry support, and other members of the Division of Analytical Bio-Medicine and the Division of Laboratory Animal Research, the Advanced Research Support Center, Ehime University. This work was supported in part by MEXT/JSPS KAKENHI (JP18H06439 and JP19K19947 to H.S.; JP23689066, JP15H04961, JP15K15552, JP17K19728, JP19H03786 to Y.I.); HIRAKU-Global Program, which is funded by MEXT's "Strategic Professional Development Program for Young Researchers" (to H.S.); and The Nakatomi Foundation and Takeda Science Foundation (to H.S. and Y.I.), UCBJ (to Y.I.) and by the Joint Usage/Research Center for Developmental Medicine, IMEG, Kumamoto University. This work was partly performed in the Cooperative Research Project Program of the Medical Institute of Bioregulation, Kyushu University.

AUTHOR CONTRIBUTIONS

Conceptualization, H.S. and Y.I.; Methodology, H.S., K.T., S.N., I.S., Y.O., S.F., and Y.O.; Software, H.S., N.T., K.T., and S.N.; Validation, H.S. and Y.S.; Formal analysis, H.S., N.T., K.T., and S.N.; Investigation,

H.S., Y.S., and N.T.; Resources, Y.O., S.F., and Y.O.; Data curation, H.S., N.T., and K.T.; Writing—original draft, H.S. and Y.I.; Writing—review & editing, H.S. and Y.I.; Visualization, H.S. and Y.S.; Supervision, H.S., T.K., T.S., and Y.I.; Project administration, Y.I.; Funding acquisition, H.S., T.K., T.S., and Y.I.

DECLARATION OF INTERESTS

The authors declare no competing interests.

Received: April 20, 2021

Revised: December 6, 2021

Accepted: February 10, 2022

Published: March 18, 2022

REFERENCES

- Bi, W., Deng, J.M., Zhang, Z., Behringer, R.R., and de Crombrugge, B. (1999). Sox9 is required for cartilage formation. *Nat. Genet.* 22, 85–89.
- Blanchart, A., Navis, A.C., Assaife-Lopes, N., Usoskin, D., Aranda, S., Sontheimer, J., and Erfors, P. (2018). UHRF1 licensed self-renewal of active adult neural stem cells. *Stem Cell.* 36, 1736–1751.
- Bostick, M., Kim, J.K., Estève, P.-O., Clark, A., Pradhan, S., and Jacobsen, S.E. (2007). UHRF1 plays a role in maintaining DNA methylation in mammalian cells. *Science* 317, 1760–1764.
- Carrió, E., Díez-Villanueva, A., Lois, S., Mallona, I., Cases, I., Forn, M., Peinado, M.A., and Suelves, M. (2015). Deconstruction of DNA methylation patterns during myogenesis reveals specific epigenetic events in the establishment of the skeletal muscle lineage. *Stem Cell.* 33, 2025–2036.
- Consortium, T.E.P., Moore, J.E., Purcaro, M.J., Pratt, H.E., Epstein, C.B., Shores, N., Adrian, J., Kawli, T., Davis, C.A., Dobin, A., et al. (2020). Expanded encyclopaedias of DNA elements in the human and mouse genomes. *Nature* 583, 699–710.
- Dobin, A., Davis, C.A., Schlesinger, F., Drenkow, J., Zaleski, C., Jha, S., Batut, P., Chaisson, M., and Gingeras, T.R. (2013). STAR: ultrafast universal RNA-seq aligner. *Bioinformatics* 29, 15–21.
- Gerli, M.F.M., Moyle, L.A., Benedetti, S., Ferrari, G., Ucuncu, E., Ragazzi, M., Constantinou, C., Louca, I., Sakai, H., Ala, P., et al. (2019). Combined Notch and PDGF signaling enhances migration and expression of stem cell markers while inducing perivascular cell features in muscle satellite cells. *Stem Cell Rep.* 12, 461–473.
- Hatazawa, Y., Ono, Y., Hirose, Y., Kanai, S., Fujii, N.L., Machida, S., Nishino, I., Shimizu, T., Okano, M., Kamei, Y., et al. (2018). Reduced Dnmt3a increases Gdf5 expression with suppressed satellite cell differentiation and impaired skeletal muscle regeneration. *Faseb J.* 32, 1452–1467.
- Iio, H., Kikugawa, T., Sawada, Y., Sakai, H., Yoshida, S., Yanagihara, Y., Ikeda, A., Saeki, N., Fukada, S., Saika, T., et al. (2021). DNA maintenance methylation enzyme Dnmt1 in satellite cells is essential for muscle regeneration. *Biochem. Biophys. Res. Commun.* 534, 79–85.
- Kim, D., Paggi, J.M., Park, C., Bennett, C., and Salzberg, S.L. (2019). Graph-based genome alignment and genotyping with HISAT2 and HISAT-genotype. *Nat. Biotechnol.* 37, 907–915.
- Lagha, M., Sato, T., Bajard, L., Daubas, P., Esner, M., Montarras, D., Relaix, F., and Buckingham, M. (2008). Regulation of skeletal muscle stem cell behavior by Pax3 and Pax7. *Cold Spring Harb. Symp. Quant. Biol.* 73, 307–315.
- Lahmann, I., Griger, J., Chen, J.-S., Zhang, Y., Schuelke, M., and Birchmeier, C. (2021). Met and Cxcr4 cooperate to protect skeletal muscle stem cells against inflammation-induced damage during regeneration. *Elife* 10, e57356.
- Lepper, C., Conway, S.J., and Fan, C.-M. (2009). Adult satellite cells and embryonic muscle progenitors have distinct genetic requirements. *Nature* 460, 627–631.
- Lepper, C., Partridge, T.A., and Fan, C.-M. (2011). An absolute requirement for Pax7-positive satellite cells in acute injury-induced skeletal muscle regeneration. *Development* 138, 3639–3646.
- Liao, Y., Smyth, G.K., and Shi, W. (2014). featureCounts: an efficient general purpose program for assigning sequence reads to genomic features. *Bioinformatics* 30, 923–930.
- Liu, L., Cheung, T.H., Charville, G.W., and Rando, T.A. (2015). Isolation of skeletal muscle stem cells by fluorescence-activated cell sorting. *Nat. Protoc.* 10, 1612–1624.
- Love, M.I., Huber, W., and Anders, S. (2014). Moderated estimation of fold change and dispersion for RNA-seq data with DESeq2. *Genome Biol.* 15, 550.
- Mademtoglou, D., Asakura, Y., Borok, M.J., Alonso-Martin, S., Mourikis, P., Kodaka, Y., Mohan, A., Asakura, A., and Relaix, F. (2018). Cellular localization of the cell cycle inhibitor Cdkn1c controls growth arrest of adult skeletal muscle stem cells. *Elife* 7, e33337.
- McCarthy, J.J., Mula, J., Miyazaki, M., Erfani, R., Garrison, K., Farooqui, A.B., Srikuea, R., Lawson, B.A., Grimes, B., Keller, C., et al. (2011). Effective fiber hypertrophy in satellite cell-depleted skeletal muscle. *Development* 138, 3657–3666.
- Meilinger, D., Fellingner, K., Bultmann, S., Rothbauer, U., Bonapace, I.M., Klinkert, W.E.F., Spada, F., and Leonhardt, H. (2009). Np95 interacts with de novo DNA methyltransferases, Dnmt3a and Dnmt3b, and mediates epigenetic silencing of the viral CMV promoter in embryonic stem cells. *EMBO Rep.* 10, 1259–1264.
- Miyata, K., Miyata, T., Nakabayashi, K., Okamura, K., Naito, M., Kawai, T., Takada, S., Kato, K., Miyamoto, S., Hata, K., et al. (2015). DNA methylation analysis of human myoblasts during in vitro myogenic differentiation: de novo methylation of promoters of muscle-related genes and its involvement in transcriptional down-regulation. *Hum. Mol. Genet.* 24, 410–423.
- Morgan, H.D., Sutherland, H.G.E., Martin, D.I.K., and Whitelaw, E. (1999). Epigenetic inheritance at the agouti locus in the mouse. *Nat. Genet.* 23, 314–318.
- Mudbhary, R., Hoshida, Y., Chernyavskaya, Y., Jacob, V., Villanueva, A., Fiel, M.I., Chen, X., Kojima, K., Thung, S., Bronson, R.T., et al. (2014). UHRF1 overexpression drives DNA hypomethylation and hepatocellular carcinoma. *Cancer Cell* 25, 196–209.
- Murphy, M.M., Lawson, J.A., Mathew, S.J., Hutcheson, D.A., and Kardon, G. (2011). Satellite cells, connective tissue fibroblasts and their interactions are crucial for muscle regeneration. *Development* 138, 3625–3637.
- Naito, M., Mori, M., Inagawa, M., Miyata, K., Hashimoto, N., Tanaka, S., and Asahara, H. (2016). Dnmt3a regulates proliferation of muscle satellite cells via p57Kip2. *PLoS Genet.* 12, e1006167.
- Obata, Y., Furusawa, Y., Endo, T.A., Sharif, J., Takahashi, D., Atarashi, K., Nakayama, M., Onawa, S., Fujimura, Y., Takahashi, M., et al. (2014). The epigenetic regulator Uhrf1 facilitates the proliferation and maturation of colonic regulatory T cells. *Nat. Immunol.* 15, 571–579.
- Ogawa, R., Ma, Y., Yamaguchi, M., Ito, T., Watanabe, Y., Ohtani, T., Murakami, S., Uchida, S., Gaspari, P.D., Uezumi, A., et al. (2014). Doublecortin marks a new population of transiently amplifying muscle progenitor cells and is required for myofiber maturation during skeletal muscle regeneration. *Development* 142, 51–61.
- Oki, S., Ohta, T., Shioi, G., Hatanaka, H., Ogasawara, O., Okuda, Y., Kawaji, H., Nakaki, R., Sese, J., and Meno, C. (2018). ChIP-Atlas: a data-mining suite powered by full integration of public ChIP-seq data. *EMBO Rep.* 19, e46255.
- Panda, D.K., Miao, D., Lefebvre, V., Hendy, G.N., and Goltzman, D. (2001). The transcription factor

SOX9 regulates cell cycle and differentiation genes in chondrocytic CFK2 cells*. *J. Biol. Chem.* 276, 41229–41236.

Ramesh, V., Bayam, E., Cernilogar, F.M., Bonapace, I.M., Schulze, M., Riemenschneider, M.J., Schotta, G., and Götz, M. (2016). Loss of Uhrf1 in neural stem cells leads to activation of retroviral elements and delayed neurodegeneration. *Gene Dev.* 30, 2199–2212.

Robinson, J.T., Thorvaldsdóttir, H., Winckler, W., Guttman, M., Lander, E.S., Getz, G., and Mesirov, J.P. (2011). Integrative genomics viewer. *Nat. Biotechnol.* 29, 24–26.

Rosenblatt, J.D., Lunt, A.I., Parry, D.J., and Partridge, T.A. (1995). Culturing satellite cells from living single muscle fiber explants. *In Vitro Cell. Dev. Biol. Anim.* 31, 773–779.

Sakai, H., Sato, T., Kanagawa, M., Fukada, S., and Imai, Y. (2020). Androgen receptor in satellite cells is not essential for muscle regenerations. *Exp. Results* 1, e21.

Sambasivan, R., Yao, R., Kissenpfennig, A., Wittenberghe, L.V., Paldi, A., Gayraud-Morel, B., Guenou, H., Malissen, B., Tajbakhsh, S., and Galy, A. (2011). Pax7-expressing satellite cells are indispensable for adult skeletal muscle regeneration. *Development* 138, 3647–3656.

Seale, P., Sabourin, L.A., Girgis-Gabardo, A., Mansouri, A., Gruss, P., and Rudnicki, M.A. (2000).

Pax7 is required for the specification of myogenic satellite cells. *Cell* 102, 777–786.

Sharif, J., Muto, M., Takebayashi, S., Suetake, I., Iwamatsu, A., Endo, T.A., Shinga, J., Mizutani-Koseki, Y., Toyoda, T., Okamura, K., et al. (2007). The SRA protein Np95 mediates epigenetic inheritance by recruiting Dnmt1 to methylated DNA. *Nature* 450, 908–912.

Shinin, V., Gayraud-Morel, B., and Tajbakhsh, S. (2009). Stem cells in regenerative medicine. *Methods Mol. Biol.* 482, 295–317.

Skarnes, W.C., Rosen, B., West, A.P., Koutourakis, M., Bushell, W., Iyer, V., Mujica, A.O., Thomas, M., Harrow, J., Cox, T., et al. (2011). A conditional knockout resource for the genome-wide study of mouse gene function. *Nature* 474, 337–342.

Teissandier, A., Servant, N., Barillot, E., and Bourc'his, D. (2019). Tools and best practices for retrotransposon analysis using high-throughput sequencing data. *Mobile DNA* 10, 52.

Tsumagari, K., Baribault, C., Terragni, J., Varley, K.E., Gertz, J., Pradhan, S., Badoo, M., Crain, C.M., Song, L., Crawford, G.E., et al. (2013). Early de novo DNA methylation and prolonged demethylation in the muscle lineage. *Epigenetics* 8, 317–332.

Xiang, H., Yuan, L., Gao, X., Alexander, P.B., Lopez, O., Lau, C., Ding, Y., Chong, M., Sun, T.,

Chen, R., et al. (2017). UHRF1 is required for basal stem cell proliferation in response to airway injury. *Cell Discov.* 3, 17019.

Yamashita, M., Inoue, K., Saeki, N., Ideta-Otsuka, M., Yanagihara, Y., Sawada, Y., Sakakibara, I., Lee, J., Ichikawa, K., Kamei, Y., et al. (2018). Uhrf1 is indispensable for normal limb growth by regulating chondrocyte differentiation through specific gene expression. *Development* 145, dev 157412.

Zhang, Y., Liu, T., Meyer, C.A., Eeckhoute, J., Johnson, D.S., Bernstein, B.E., Nussbaum, C., Myers, R.M., Brown, M., Li, W., et al. (2008). Model-based analysis of ChIP-seq (MACS). *Genome Biol.* 9, R137.

Zhao, J., Chen, X., Song, G., Zhang, J., Liu, H., and Liu, X. (2017). Uhrf1 controls the self-renewal versus differentiation of hematopoietic stem cells by epigenetically regulating the cell-division modes. *Proc. Natl. Acad. Sci.* 114, E142–E151.

Zhou, Y., Zhou, B., Pache, L., Chang, M., Khodabakhshi, A.H., Tanaseichuk, O., Benner, C., and Chanda, S.K. (2019). Metascape provides a biologist-oriented resource for the analysis of systems-level datasets. *Nat. Commun.* 10, 1523.

Zhu, L.J., Gazin, C., Lawson, N.D., Pagès, H., Lin, S.M., Lapointe, D.S., and Green, M.R. (2010). ChIPpeakAnno: a bioconductor package to annotate ChIP-seq and ChIP-chip data. *BMC Bioinf.* 11, 237.

STAR★METHODS

KEY RESOURCES TABLE

| REAGENT or RESOURCE | SOURCE | IDENTIFIER |
|--|---------------------------|-----------------------------------|
| Antibodies | | |
| Mouse monoclonal anti-Pax7 | DSHB | cat# PAX7; RRID: AB_528428 |
| Rabbit polyclonal anti-Pax7 | Invitrogen | cat# PA1-117; RRID: AB_2539886 |
| Rabbit monoclonal anti-MyoD | Abcam | cat# ab133627; RRID: AB_2890928 |
| Mouse monoclonal anti-Myogenin | Santa Cruz Biotechnology | cat# sc-12732; RRID: AB_627980 |
| Mouse monoclonal anti-Uhrf1 | Santa Cruz Biotechnology | cat# sc-373750; RRID: AB_10947236 |
| Rat monoclonal anti-Uhrf1 | MBL | cat# D289-3; RRID: AB_10597260 |
| Mouse monoclonal anti-Myh1 | DSHB | cat# MF20; RRID: AB_2147781 |
| Mouse monoclonal anti-Myh3 | DSHB | cat# F1.652; RRID: AB_528358 |
| Rabbit polyclonal anti-Ki67 | Novus | cat# NB500-170; RRID: AB_10001977 |
| Rabbit monoclonal anti-Gapdh | Cell Signaling Technology | cat# 5174; RRID: AB_10622025 |
| Rat monoclonal anti-CD31-FITC | BioLegend | cat# 102406; RRID: AB_312901 |
| Rat monoclonal anti-CD45-FITC | BioLegend | cat# 103108; RRID: AB_312973 |
| Rat monoclonal anti-Sca1-APC | BioLegend | cat# 122512; RRID: AB_756197 |
| Rat monoclonal anti-Vcam1-PE | Invitrogen | cat# 12-1061-82; RRID: AB_2572573 |
| Alexa fluor 568 goat anti-mouse IgG1 | Invitrogen | cat# A-21124; RRID: AB_2535766 |
| Alexa fluor 488 goat anti-rabbit IgG | Invitrogen | cat# A-11008; RRID: AB_143165 |
| Alexa fluor 488 goat anti-rat IgG | Invitrogen | cat# A-11006; RRID: AB_2534074 |
| anti-mouse immunoglobulin/HRP | Promega | cat# W4021; RRID: AB_430834 |
| anti-rabbit immunoglobulin/HRP | Agilent | cat# P0448; RRID: AB_2617138 |
| Chemicals, peptides, and recombinant proteins | | |
| Cardiotoxin | Latoxan | cat# L8102 |
| Tamoxifen | Sigma | cat# T5648 |
| Corn oil | Sigma | cat# C8267 |
| Collagenase type 2 | Worthington | cat# LS004177 |
| Dispase | Gibco | cat# 17105-041 |
| 1% chicken embryo extract | US Biological | cat# C3999 |
| bFGF | Wako | cat# 062-06661 |
| EdU | Invitrogen | cat# A10044 |
| Critical commercial assays | | |
| ECL Prime Western Blotting Detection Reagents | Amersham | cat# RPN2232 |
| Lipofectamine RNAiMAX | Thermo Scientific | cat# 13778-075 |
| Click-iT EdU Imaging Kits | Invitrogen | cat# C10340 |
| RNeasy Plus Micro Kit | Qiagen | cat# 74034 |
| PrimeScript | Takara | cat# RR036A |
| TB Green Premix Ex Taq II | Takara | cat# RR820S |
| Agilent 2100 Bioanalyzer with RNA 6000 Pico Kit | Agilent | cat# 5067-1513 |
| NEBNext Ultra II Directional RNA Library Prep Kit for Illumina | NEB | cat# E7760S |
| NEBNext rRNA Depletion Kit | NEB | cat# E6310L |
| NEBNext Multiplex Oligos for Illumina | NEB | cat# E7335S |
| Agilent 2100 Bioanalyzer with DNA 1000 kit | Agilent | cat# 5067-1504 |
| KAPA Library Quantification Kits | KAPA Bio | cat# KK4824 |

(Continued on next page)

Continued

| REAGENT or RESOURCE | SOURCE | IDENTIFIER |
|--|----------------|----------------|
| NucleoSpin Tissue Kit | MACHEREY-NAGEL | cat# 740952 |
| EpiXplore Methylated DNA Enrichment Kit | Clontech | cat# PT5034-2 |
| DNA SMART CHIP-Seq Kit | Takara | cat# 634865 |
| E-Gel 2% SizeSelect electrophoresis | Invitrogen | cat# G661012 |
| Agilent 2100 Bioanalyzer with the High Sensitivity DNA kit | Agilent | cat# 5067-4626 |

Deposited data

| | | |
|--|-------------------------|---|
| Raw and analyzed data | This paper | GEO: GSE169193 |
| Mouse reference genome GRCm38, PRI | GENCODE | https://www.encodegenes.org/mouse/ |
| Proximal enhancer-like (pELS) bed file | Consortium et al., 2020 | https://screen.encodeproject.org |
| H3K4me1 peaks of MC3T3-E1 | Oki et al., 2018 | http://chip-atlas.org |

Experimental models: Cell lines

| | | |
|--------------------|------|----------|
| Mouse: C2C12 cells | ATCC | CRL-1772 |
|--------------------|------|----------|

Experimental models: Organisms/strains

| | | |
|--|------------------------|-------------|
| Mouse: Pax7 ^{CE/+} ; B6;129-Pax7 ^{tm2.1(cre/ERT2)Fan/J} | The Jackson Laboratory | JAX: 012476 |
| Mouse: Uhrf1 ^{fl/fl} ; B6Dnk; B6N-Uhrf1 ^{<tm1a(EUCOMM)Wtsi>/leg} | The EUCOMM program | MGI:4434100 |

Oligonucleotides

| | | |
|---|------------|-----------------------|
| non-targeting siRNA | Dharmacon | cat# D-001810-10-05 |
| siRNA targeting Sox9 | Dharmacon | cat# L-059108-01-0005 |
| Primers for Uhrf1, see Table S2 | This paper | NA |
| Primers for MyoD1, see Table S2 | This paper | NA |
| Primers for Myog, see Table S2 | This paper | NA |
| Primers for Sox9, see Table S2 | This paper | NA |

Software and algorithms

| | | |
|---------------------------------------|---|---|
| Fiji (v2.3.0) | Schneider et al., 2012 | https://imagej.net/Fiji |
| TrimGalore (v0.6.6) | https://github.com/FelixKrueger/TrimGalore | http://www.bioinformatics.babraham.ac.uk/projects/trim_galore/ |
| HISAT2 (v2.2.1) | Kim et al., 2019 | http://daehwankimlab.github.io/hisat2/ |
| DESeq2 (v1.30.1) | Love et al., 2014 | https://bioconductor.org/packages/release/bioc/html/DESeq2.html |
| Metascape | Zhou et al., 2019 | http://metascape.org |
| STAR (v2.7.6a) | Dobin et al., 2013 | https://github.com/alexdobin/STAR |
| featureCounts (v2.0.1) | Liao et al., 2014 | http://subread.sourceforge.net |
| MACS2 (v2.2.6) | Zhang et al., 2008 | https://github.com/macs3-project/MACS/tree/release_v2.2.6 |
| ChIPpeakAnno (v3.24.2) | Zhu et al., 2010 | https://bioconductor.org/packages/release/bioc/html/ChIPpeakAnno.html |
| Prism (v9.3.1) | GraphPad | https://www.graphpad.com/scientific-software/prism/ |
| R (v4.0.5) | R Core Team 2020 | https://www.r-project.org/ |
| Integrative Genomics Viewer (v2.11.4) | Robinson et al., 2011 | https://igv.org |
| FlowJo (v10.1r7) | BD Life Sciences | https://www.flowjo.com |

RESOURCE AVAILABILITY

Lead contact

Further information and requests for resources and reagents should be directed to and will be fulfilled by the lead contact, Yuuki Imai (y-imai@m.ehime-u.ac.jp).

Materials availability

This study did not generate new unique reagents.

Data and code availability

- RNA-Seq and MBD2-Seq data have been deposited in the Gene Expression Omnibus as accession number GSE169193 and are publicly available as of the date of publication.
- This paper does not report original code.
- Any additional information required to reanalyze the data reported in this paper is available from the lead contact upon request.

EXPERIMENTAL MODEL AND SUBJECT DETAILS

Animals

All animals were maintained and used according to a protocol approved by the Animal Experiment Committee of Ehime University, Japan. C57BL/6Jcl mice were purchased from CLEA Japan. The *Pax7^{CE/+}* (Lepper et al., 2009); Jackson Laboratories, stock no: 012476) and *Uhrf1^{fl/fl}* (B6Dnk;B6N-Uhrf1^{<tm1a(EUCOMM)Wtsi>/leg} (Skarnes et al., 2011)); mouse strains have been described previously. *Uhrf1^{fl/fl}* mice were crossed with *Pax7^{CE/+}* mice to generate *Pax7^{CE/+};Uhrf1^{fl/fl}* mice. All mice were housed in a specific pathogen-free facility under climate-controlled conditions and a 12-h light/dark cycle and were provided water and a standard diet *ad libitum*. All male animals were evaluated at age 7–12 weeks old. At 7 weeks of age, tamoxifen (150 μ L, 20 mg/mL) (Sigma, cat# T5648) dissolved in corn oil (Sigma, cat# C8267) was injected intraperitoneally for 5 consecutive days to induce Cre-mediated recombination. After 1 week of tamoxifen injection, injury was induced by injecting 100 μ L of 10 μ M cardiotoxin (CTX) solution (Latoxan, cat# L8102) into the left tibialis anterior (TA) muscles under anesthesia using isoflurane. The right TA served as the intact control.

Cell lines

The C2C12 cell line (female, ATCC, CRL-1772) was culture in DMEM (Gibco, cat# 10569-010) supplemented with 10% FBS (Gibco, cat# 10099-141) and antibiotic–antimycotic (Gibco, cat# 15240-062) in a 37°C incubator with 5% CO₂. The medium was replaced with differentiation medium (DMEM supplemented with 2% horse serum) to induce myotube formation.

Primary cell cultures

Isolated skeletal muscle-derived mononuclear myogenic cells from male mice were resuspended in DMEM/F12 (Gibco, cat# 10565-018) supplemented with 20% FBS, 2% Ultrosor G (Pall, cat# 15950-017), and antibiotic–antimycotic in a 37°C incubator with 5% CO₂. Cells at 5000 or 10000/cm² were cultured on an 8-well chamber slide (Thermo Scientific, cat# 177445) or in a 6-well plate coated with 1 mg/ml Matrigel (Corning, cat# 354230). Please see the following sections for more information on isolation methods.

METHOD DETAILS

Immunofluorescence and microscopy

For immunofluorescence (IF) staining, muscles were frozen in liquid nitrogen-chilled isopentane, and 10 μ m cryosections were prepared. For Pax7 and Uhrf1 staining, sections were fixed in 4% paraformaldehyde (PFA) in PBS for 5 min and then boiled in antigen retrieval buffer (10 mM sodium citrate, pH 6) for 10 min. For Myh3 staining, tissue sections were fixed for 10 min in acetone at –20 °C before boiling, blocked in 5% goat serum (Gibco, cat# 16210-064) in PBS for 60 min, and incubated with the primary antibodies overnight at 4°C. The antibodies used for IF staining were anti-Pax7 (DSHB, cat# PAX7, RRID: AB_528428; 1/5 dilution; or Invitrogen, cat# PA1-117, RRID: AB_2539886; 1/100 dilution), anti-MyoD (Abcam, cat# ab133627, RRID: AB_2890928; 1/100 dilution), anti-Uhrf1 (Santa Cruz Biotechnology, cat# sc-373750, RRID: AB_10947236; 1/50 dilution), anti-Myh3 (DSHB, cat# F1.652, RRID: AB_528358; 1/20 dilution), Alexa fluor 568 goat anti-mouse IgG1 (Invitrogen, cat# A-21124; RRID: AB_2535766; 1/1000 dilution), and Alexa fluor 488 goat anti-rabbit IgG (Invitrogen, cat# A-11008; RRID:AB_143165; 1/1000 dilution).

For IF staining in cells, cells were fixed in 4% PFA in PBS for 10 min, followed by permeabilization using 0.5% Triton X-100 in PBS for 10 min. Cells were blocked using 5% goat serum in PBS. The following primary antibodies were used: anti-Uhrf1 (Santa Cruz Biotechnology, cat# sc-373750, RRID: AB_10947236; 1/100

dilution; or MBL, cat# D289-3 RRID: AB_10597260; 1/100 dilution), anti-Ki67 (Novus, cat# NB500-170, RRID: AB_10001977; 1/100 dilution), anti-Myogenin (Santa Cruz Biotechnology, cat# sc-12732, RRID: AB_627980; 1/100 dilution), and anti-Myh1 (DSHB, cat# MF20, RRID: AB_2147781; 1/10 dilution). The signals were visualized using the following fluorochrome-coupled secondary antibodies: Alexa fluor 568 goat anti-mouse IgG1a, Alexa fluor 488 goat anti-rabbit IgG, and Alexa fluor 488 goat anti-rat IgG (Invitrogen, cat# A-11006, RRID: AB_2534074; 1/1000 dilution). Nuclei were counterstained with DAPI.

Stained cells or tissues were photographed using BIOREVO (Keyence) and quantified using Fiji (v2.3.0) (<https://imagej.net/Fiji>). The numbers of Uhrf1+, Pax7+, Ki67+, Myogenin+, and EdU+ cells *in vitro* and the area of Myh3+ fibers *in vivo* were determined using the Fiji Analyze Particles function. For total muscle CSA quantification, the whole area of transverse TA muscle sections was measured by laminin staining. The numbers of Uhrf1+, Pax7+, MyoD+, and EdU+ cells *in vivo* were determined by manual counting using the Adobe Photoshop count tool.

Isolation of skeletal muscle-derived mononuclear myogenic cells

Isolation of mononuclear myogenic cells from hindlimb muscles was performed as described (Liu et al., 2015) with minor modifications. Briefly, muscles were chopped in cold PBS and digested using 800 U/mL collagenase type 2 (Worthington, cat# LS004177) in F10 medium (Gibco, cat# 11550-043) supplemented with horse serum (Gibco, cat# 26050-088) and antibiotic-antimycotic (Gibco, cat# 15240-062) for 60 min followed by another digestion using 1000 U/mL collagenase type 2 and 11 U/mL dispase (Gibco, cat# 17105-041) for 30 min. The supernatants were filtered through a 40 μ m cell strainer (Falcon, cat# 352340) and centrifuged to yield a cell suspension. The following antibodies were used: CD31-FITC (BioLegend, cat# 102406; RRID: AB_312901; 1/100 dilution), CD45-FITC (BioLegend, cat# 103108, RRID: AB_312973; 1/100 dilution), Sca1-APC (BioLegend, cat# 122512, RRID: AB_756197; 1/100 dilution), and Vcam1-PE (Invitrogen, cat# 12-1061-82, RRID: AB_2572573; 1/100 dilution). Cells were isolated using the FACS Aria II (Becton, Dickinson and Company) and analyzed by FlowJo v10.1r7 (BD Life Sciences).

Western blotting

Cultured myogenic cells were washed with PBS and dissolved in RIPA buffer (FUJIFILM, cat# 182-02451) containing protease inhibitors (nacalai tesque, cat# 25,955-11). Whole-cell extracts were separated by SDS-PAGE and transferred to polyvinylidene fluoride membranes. The membranes were blocked with 5% skim milk in TBS with Tween-20 (PBST), followed by incubation with an anti-Uhrf1 antibody (Santa Cruz Biotechnology, cat# sc-373750, RRID: AB_10947236; 1/500 dilution) or anti-Gapdh antibody (Cell Signaling Technology, cat# 5174, RRID: AB_10622025; 1/1000 dilution) overnight at 4 °C. After washing with PBST, the membranes were incubated with an anti-mouse (Promega, cat# W4021, RRID: AB_430834; 1:5000) or anti-rabbit immunoglobulin/HRP secondary antibody (Agilent, cat# P0448, RRID: AB_2617138; 1:5000) for 60 min at room temperature. Immunoreactive signals were detected using ECL Prime Western Blotting Detection Reagents (Amersham, cat# RPN2232) on the Image Quant LAS 4000 system (GE Healthcare).

siRNA transfection

Cells were transfected with non-targeting siRNA (Dharmacon, cat# D-001810-10-05) or siRNA targeting Sox9 (Dharmacon, cat# L-059108-01-0005) using Lipofectamine RNAiMAX (Thermo Scientific, cat# 13778-075) following the manufacturer's protocol.

EdU labelling and detection

For *in vivo* labelling, EdU (5-ethynyl-2'-deoxyuridine, Invitrogen, cat# A10044) was dissolved in PBS at 0.5 μ g/ μ L and injected intraperitoneally into mice at 5 μ g/g body weight 24 h before harvesting. For *in vitro* labelling, the cells were incubated with EdU (10 μ M) for 3 h. EdU was detected using Click-iT EdU Imaging Kits (Invitrogen, cat# C10340) with Alexa Flour 647.

RNA isolation and quantitative real-time PCR

Total RNA was extracted from 3 day cultured myogenic cells using the RNeasy Plus Micro Kit (Qiagen, cat# 74034) following the manufacturer's protocol. cDNA was synthesized from total RNA using PrimeScript (Takara, cat# RR036A). qPCR was performed in duplicate samples using TB Green Premix Ex Taq II (Takara, cat# RR820S) and Thermal Cycler Dice (Takara, cat# TP850). The primer sequences are listed in Table S2.

Isolation, culture, and immunostaining of single myofibers

Single myofibers were isolated from extensor digitorum longus (EDL) muscles as described previously (Rosenblatt et al., 1995). Briefly, EDL muscles were mildly digested with 0.2% collagenase type 2 in DMEM for 90 min at 37°C. The isolated fibers were cultured in DMEM supplemented with 30% FBS, 1% chicken embryo extract (US Biological, cat# C3999), and 10 ng/mL bFGF (Wako, cat# 062-06661). Immunostaining was performed following a previous protocol (Shinin et al., 2009). The isolated fibers were fixed in 4% PFA in PBS for 10 min and then blocked using 5% goat serum in PBS for 30 min. The antibodies used for IF staining were anti-Pax7 (DSHB, cat# PAX7, RRID: AB_528428; 1/5 dilution) and anti-MyoD (Abcam, cat# ab133627, RRID: AB_2890928; 1/100 dilution).

RNA-Seq and data analysis

The integrity of isolated RNA was verified using the Agilent 2100 Bioanalyzer with RNA 6000 Pico Kit (Agilent, cat# 5067-1513). RNA-Seq libraries were prepared using the NEBNext Ultra II Directional RNA Library Prep Kit for Illumina (NEB, cat# E7760S) with the NEBNext rRNA Depletion Kit (NEB, cat# E6310L) and NEBNext Multiplex Oligos for Illumina (NEB, cat# E7335S) according to the manufacturer's instructions. The constructed libraries were verified using the Agilent 2100 Bioanalyzer with DNA 1000 kit (Agilent, cat# 5067-1504) and quantified using KAPA Library Quantification Kits (KAPA Bio, cat# KK4824) and the 7500 Real-Time PCR System (ABI, cat# 7500-01). The libraries were sequenced as 50 or 150 bp paired-end reads using the HiSeq 1500 or NovaSeq 6000 Sequencing System (Illumina), respectively. Raw reads were trimmed using TrimGalore (v0.6.6; http://www.bioinformatics.babraham.ac.uk/projects/trim_galore/) and mapped to the reference genome (GRCm38, PRI) using HISAT2 (v2.2.1) (Kim et al., 2019). The option '-trim3 99' was used to compare reads of different lengths. Expression level was quantified using featureCounts (v2.0.1) (Liao et al., 2014) with GRCm38.102 annotation. The differentially expressed genes were extracted by DESeq2 (v1.30.1) (Love et al., 2014). GO enrichment analysis was performed using Metascape (Zhou et al., 2019).

For transposable element (TE) analysis, raw reads were trimmed using TrimGalore and mapped to the reference genome (GRCm38, PRI, <https://www.gencodegenes.org/mouse/>) using STAR (v2.7.6a; Dobin et al., 2013) with the PRI annotation. For the mapping, the STAR option '-runMode alignReads -runThreadN 4 -outMultimapperOrder Random -outSAMtype BAM SortedByCoordinate -outSAMmultNmax 1 -outFilterMultimapNmax 1000 -outFilterMismatchNmax 3 -winAnchorMultimapNmax 1000 -alignIntronMax 1 -alignMatesGapMax 350 -alignEndsType EndToEnd' was used, allowing a higher number of multi-mapped reads (Teissandier et al., 2019). TE families were quantified using featureCounts (v2.0.1; -M -T 1 -s 0 -p) and TE annotation (http://labshare.cshl.edu/shares/mhammellab/www-data/TEtranscripts/TE_GTF/). The differentially expressed TEs were extracted by DESeq2.

MBD2-Seq and analysis of the sequencing data

Genomic DNA was isolated and purified using the NucleoSpin Tissue Kit (MACHEREY-NAGEL, cat# 740952). Purified DNA was sheared using the Covaris S220 ultrasonicator with microTUBE AFA (Covaris, cat# 520045). Methylated and non-methylated DNA fragments were separated using the EpiXplore Methylated DNA Enrichment Kit (Clontech, cat# PT5034-2). Libraries were generated using the DNA SMART CHIP-Seq Kit (Takara, cat# 634865). The libraries were selected from 250 to 350-bp fragments obtained by E-Gel 2% SizeSelect electrophoresis (Invitrogen, cat# G661012). Size-selected libraries were verified using the Agilent 2100 Bioanalyzer with the High Sensitivity DNA kit (Agilent, cat# 5067-4626) and quantified using KAPA Library Quantification Kits (KAPA Bio, cat# KK4824) and the 7500 Real-Time PCR System (ABI, cat# 7500-01). The libraries were sequenced using NovaSeq 6000 with 150 bp paired end reads. Raw reads were down-sampled to 50 million reads for each condition to avoid the bias due to different sequencing depths. The reads were trimmed using TrimGalore and were mapped using HISAT2. Peaks were obtained by MACS2 (v2.2.6) (Zhang et al., 2008) using cells derived from TMX-treated mice as the 'control,' with the following options: '-slocal 0 -llocal 0 -q 0.01'. ChIPpeakAnno (v3.24.2) (Zhu et al., 2010) was used to annotate and visualize the peaks. Methylated DNA signals were visualized using Integrative Genomics Viewer (IGV) (Robinson et al., 2011). We downloaded the Proximal enhancer-like (pELS) bed file for mouse from the SCREEN portal (Consortium et al., 2020) (<https://screen.encodeproject.org>). H3K4me1 peaks of MC3T3-E1 was downloaded from CHIP-Atlas web tools (Oki et al., 2018) (<http://chip-atlas.org>).



QUANTIFICATION AND STATISTICAL ANALYSIS

The scatterplot with means are used to show values. In a bar chart, values are expressed as means \pm SD (Figure S3B) or 95% CI (Figures 1 and S1B). The exact values of n are indicated in the corresponding figure legends. Two-sample test for equality of proportions was performed by Test of Equal or Given Proportions. Welch's t-test was used to compare variable between two groups. Welch's ANOVA with Dunnett's T3 multiple comparison test was used to compare variables among three or more. Data were analyzed using Prism 9 (GraphPad Software) or R (v4.0.5) (<https://www.r-project.org>). Statistical significance was set at $p < 0.05$.